

# SCIENTIFIC REPORTS



OPEN

## Gas sensors boosted by two-dimensional h-BN enabled transfer on thin substrate foils: towards wearable and portable applications

Taha Ayari<sup>1,2</sup>, Chris Bishop<sup>3</sup>, Matthew B. Jordan<sup>1,2</sup>, Suresh Sundaram<sup>4</sup>, Xin Li<sup>1</sup>, Saiful Alam<sup>1,2</sup>, Youssef ElGmili<sup>1</sup>, Gilles Patriarche<sup>5</sup>, Paul L. Voss<sup>1,2</sup>, Jean Paul Salvestrini<sup>1,2</sup> & Abdallah Ougazzaden<sup>1,2</sup>

The transfer of GaN based gas sensors to foreign substrates provides a pathway to enhance sensor performance, lower the cost and extend the applications to wearable, mobile or disposable systems. The main keys to unlocking this pathway is to grow and fabricate the sensors on large h-BN surface and to transfer them to the flexible substrate without any degradation of the performances. In this work, we develop a new generation of AlGaIn/GaN gas sensors with boosted performances on a low cost flexible substrate. We fabricate 2-inch wafer scale AlGaIn/GaN gas sensors on sacrificial two-dimensional (2D) nano-layered h-BN without any delamination or cracks and subsequently transfer sensors to an acrylic surface on metallic foil. This technique results in a modification of relevant device properties, leading to a doubling of the sensitivity to NO<sub>2</sub> gas and a response time that is more than 6 times faster than before transfer. This new approach for GaN-based sensor design opens new avenues for sensor improvement via transfer to more suitable substrates, and is promising for next-generation wearable and portable opto-electronic devices.

AlGaIn/GaN-based sensors with catalytically active gate electrodes are an interesting sensing technology due to their many advantageous material properties, such as high thermal and chemical stability<sup>1</sup>, which have demonstrated sensitivity and suitability for detection of diesel exhaust gases<sup>2,3</sup>. With appropriate transfer technique, AlGaIn/GaN sensors have promising potential to be integrated into wearable applications. This would enable the development of a wearable and portable air pollutant monitoring platform to collect air pollutant data (species and concentration) continuously. Such a system requires inexpensive, miniaturized (micro-scale), rapidly responding and highly sensitive gas sensors that can be operated on malleable and lightweight substrates. Existing Metal Organic Vapour Phase Epitaxy (MOVPE) for GaN-based sensors uses fabrication on a rigid substrate, typically sapphire or silicon, and epi-layers cannot be easily released from the substrate because of the strong bonding. Several options for the release of epi-layers exist including fielded laser lift-off<sup>4</sup> for GaN devices and chemical etching of the growth substrate<sup>5</sup> or a sacrificial layer<sup>6</sup>. These techniques have many limitations in practice, notably high cost, long process times, and limitations in size.

Van der Waals epitaxy, which involves the growth of sp<sup>3</sup> bonded semiconductor layers on 2D materials<sup>7</sup>, allows active layer release from its substrate and transfer to a foreign support<sup>8,9</sup>. This promises to reduce manufacturing cost by permitting re-use of the native substrate. It can also enable device integration into low-cost substrate foils, which can be used for foldable, wrapped, rollable and portable systems<sup>10</sup>. Hexagonal boron nitride (h-BN) is a III-N material which exhibits a two-dimensional structure when grown as monolayers of nanometer thicknesses, similar to graphene. It is particularly compatible with growth of wurtzite III-N devices in a single growth run. AlGaIn/GaN HEMT and InGaIn-based LEDs have been grown and fabricated on h-BN<sup>11,12</sup>, but large-scale device fabrication has not been yet demonstrated.

<sup>1</sup>CNRS, UMI 2958, GT - CNRS, 2 rue Marconi, 57070, Metz, France. <sup>2</sup>Georgia Institute of Technology, School of Electrical and Computer Engineering, GT-Lorraine, 57070, Metz, France. <sup>3</sup>Institut Lafayette, 57070, Metz, France. <sup>4</sup>GT Lorraine, UMI 2958, GT - CNRS, 2 rue Marconi, 57070, Metz, France. <sup>5</sup>Centre de Nanosciences et de Nanotechnologies, CNRS, Univ. Paris-Sud, Université Paris-Saclay, C2N – Marcoussis, 91460, Marcoussis, France. Correspondence and requests for materials should be addressed to A.O. (email: [aougazza@georgiatech-metz.fr](mailto:aougazza@georgiatech-metz.fr))

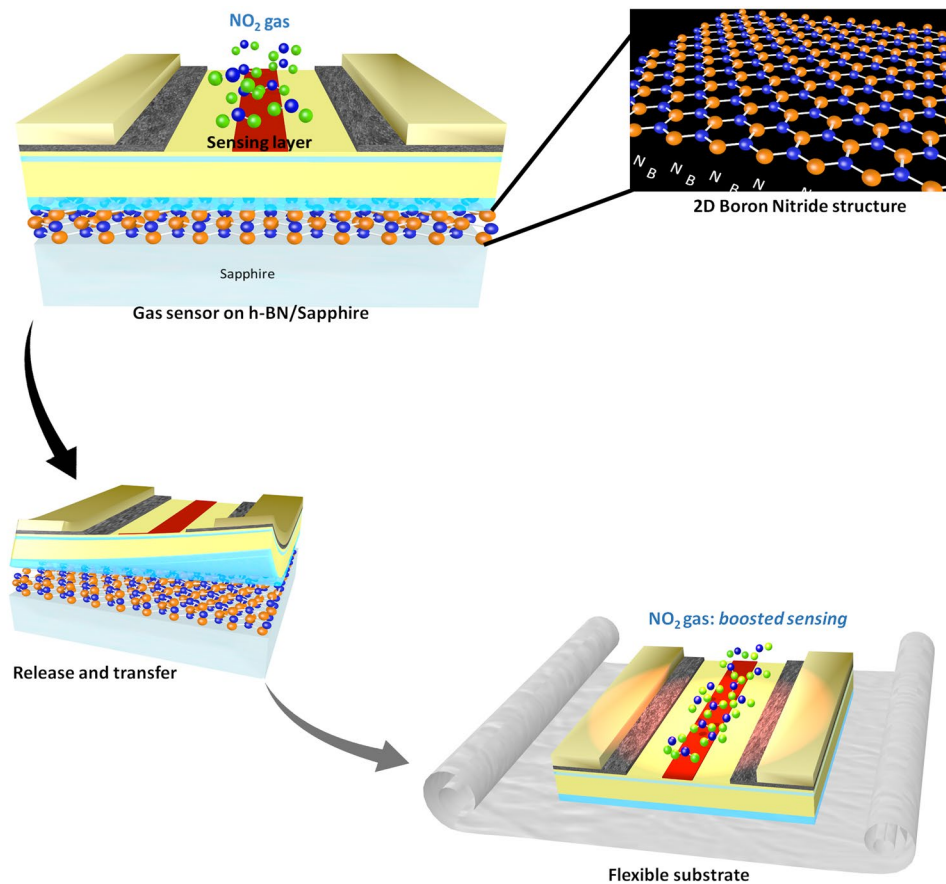


**Figure 1.** Our approach for the growth, fabrication, release and transfer (see Method section for details) of boosted AlGaIn/GaN gas sensor to a flexible sheet using h-BN as a buffer and release layer.

In this work, we report wafer-scale fabrication of AlGaIn/GaN gas sensors grown on 2-inch sapphire wafers with a sacrificial 2D layered h-BN by MOVPE. In addition to transferring sensor devices to a flexible substrate, we demonstrate an enhancement in gas sensing performance of these devices. This is in part due to the effect of foreign substrate choice on the temperature in the two-dimensional gas (2DEG) channel of the AlGaIn/GaN heterostructure, which is validated by thermal modeling and Raman spectroscopy. We also analyze the strain changes in the semiconductor materials after release from the sapphire layer, and consider its effect on device performance. The sensors are tested before and after transfer to the flexible substrate with significant improvements in both sensitivity and response time after the transfer. This approach for engineering of GaN-based sensors is a key step in the pathway towards economically viable, flexible sensors with improved performances that could be integrated into wearable applications.

The mechanism for boosted gas sensor operating on a foreign substrate like a flexible carrier is illustrated in Fig. 1. The 2D h-BN (the crystallographic phase of the grown h-BN has been demonstrated in a previous study<sup>13</sup>) layer enables the release of the device and its transfer to an acrylic adhesive layer. This layer is expected to confine the heat generated by self-heating, leading to higher operating temperature of the gas sensor, which is known to contribute to an increase of the sensitivity and an improvement of the response time<sup>2</sup>.

**Structural characterization of AlGaIn/GaN structure on sapphire.** The AlGaIn/GaN structure was grown by MOVPE on 2-inch h-BN/sapphire substrates (Fig. 2a). The high-resolution X-ray diffraction (HRXRD)  $2\theta - \omega$  scan of the grown layers on h-BN/sapphire is presented in Fig. 2b. The satellite peaks from the  $\text{Al}_{0.25}\text{Ga}_{0.75}\text{N}/\text{GaN}$  heterostructure were clearly observed, along with GaN (002) and  $\text{Al}_{0.14}\text{Ga}_{0.86}\text{N}$  (002) diffraction planes. Simulation, shown in blue, confirms the Al content and the thicknesses of the different layers in the structure. The broadness and the low intensity of the AlGaIn buffer compared to the simulated one are due to the 3D morphology of this layer as shown in the elemental EDX mapping of Al in Fig. 2d. The high resolution TEM image in Fig. 2c is a direct evidence of the crystal phase and quality of the 5 nm thick h-BN layer. An abrupt interface without inter-diffusion along the  $\text{Al}_{0.25}\text{Ga}_{0.75}\text{N}/\text{GaN}$  can be seen in energy dispersive X-ray spectroscopy (EDX) element mapping in Fig. 2d.

**Electrical characterization of AlGaIn/GaN devices on sapphire.** The process fabrication has been adapted for device structures on 2D h-BN. For instance, no ultrasonic cleaning is used, rapid thermal annealing conditions such as gas flow rate and temperature ramping were optimized, and contact with liquids was limited

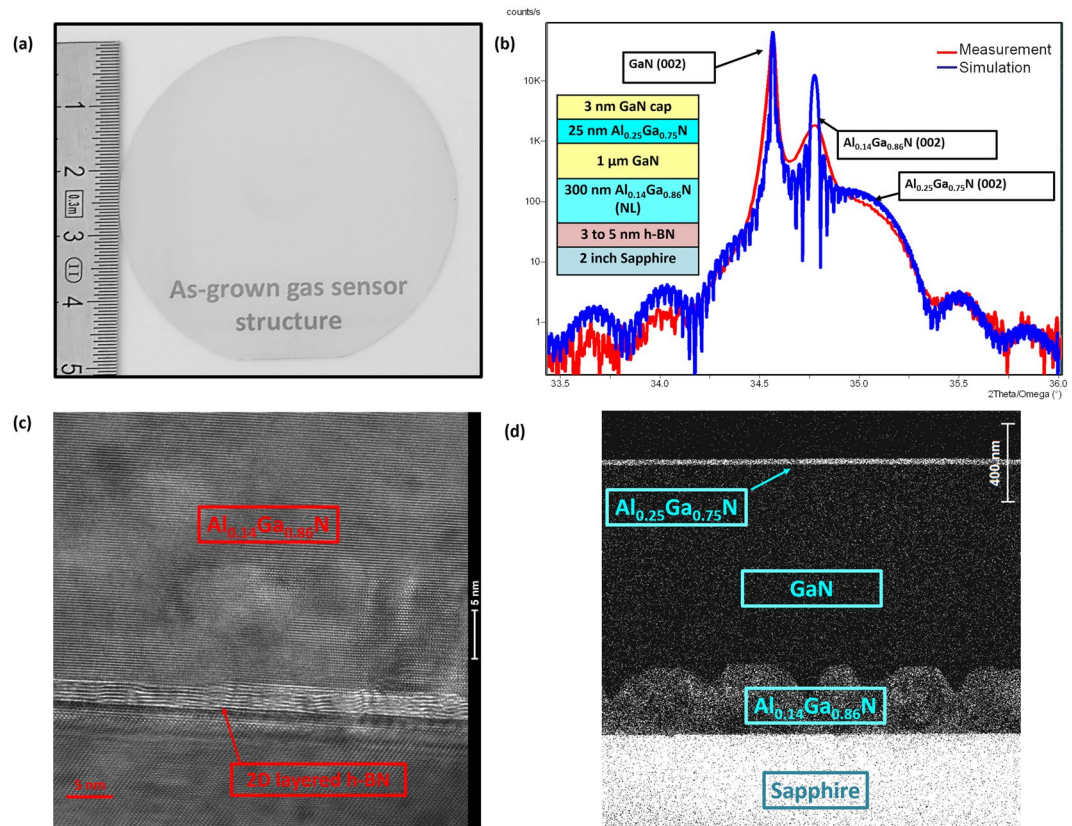


**Figure 2.** (a) Photo of the grown AlGaN/GaN on h-BN, (b) High resolution X-ray diffraction  $2\theta - \omega$  scans of the grown AlGaN/GaN heterostructure on h-BN using  $\text{Al}_{0.14}\text{Ga}_{0.86}\text{N}$  as a nucleation layer (NL), the red curve is the measurement and the blue curve presents the simulation result. The inset is a schematic of the grown structure. (c) High resolution TEM image showing the interface between the 2D layered h-BN and the AlGaN nucleation layer. (d) Energy dispersive X-ray spectroscopy (EDX) elemental mapping of Al.

during each step to prevent spontaneous delamination<sup>14</sup>. The resulting processed device is shown in Fig. 3a. Transfer length measurements (TLM) performed on several locations of the wafer show an average specific contact resistivity of  $3 \times 10^{-5} \Omega \cdot \text{cm}^{-2}$ , indicating good ohmic contact behavior. Wafer mapping of the current-voltage characteristics reveal more than 1000 functional AlGaN/GaN devices on the 2-inch wafer (Fig. 3b,c); processing optimizations can further improve the yield. We also note that more than 100 devices exhibit more than 70% gate pinching, which we have quantified as  $[(I_{\text{ds}}(V_{\text{gs}} = 0 \text{ V}) - I_{\text{ds}}(V_{\text{gs}} = -6 \text{ V})/I_{\text{ds}}(V_{\text{gs}} = 0 \text{ V})] * 100$  at  $V_{\text{ds}} = 10 \text{ V}$ . This is a direct indication that these devices have good control of the carrier concentration in the 2DEG by the gate contact (Fig. 3d).

**Sensor measurements: before and after transfer.** AlGaN/GaN gas sensors with greater than 80% gate pinching were tested under  $\text{NO}_2$  gas for a concentration of 100 ppm at  $30^\circ\text{C}$ , both as-grown on the original sapphire substrate and after transfer to a tape with acrylic adhesive. Exposure to the gas leads to decreased drain-source current. From the transient response and recovery curves, we have calculated sensitivity as  $S = [(I_0 - I_{\text{gas}})/I_0] * 100$ , where  $I_0$  is the initial current under pure  $\text{N}_2$  and  $I_{\text{gas}}$  is the steady state current after the test gas has been applied. This metric gives a normalized measure of the change in device current under gas exposure. We have also determined the response time  $\tau$  defined by the time between 10% and 90% of the initial and final steady state values under gas exposure. The average sensitivity  $S$  was found to be  $2.8\% \pm 1.4\%$  with an average response time of  $361 \text{ s} \pm 140.8 \text{ s}$  for around 20 tested devices. Figure 4a presents one of the best response we obtained before the transfer,  $S$  and  $\tau$  were calculated to be equal to 6.5% and 385 s respectively. Working devices after the transfer to the new substrate have undergone the same testing procedure. The results indicate an average sensitivity  $S = 12\% \pm 1.2\%$  with a response time ranging from 7 s to 61 s. Figure 4b shows result from the same device, used in Fig. 4a, after its transfer. This sensor presents a doubling in sensitivity, a six times lower response time and a faster recovery after gas exposure. We also note that a repeated measurement with 9 test cycles during more than three consecutive hours has been performed after the transfer exhibiting similar response and no significant drift, as shown in Fig. 4c.

The observed large enhancement in sensitivity and response time after transfer may be attributed to several root causes. Our choice of the final support is expected to enable the confinement of the heat generated by self-heating. As seen in Fig. 5, thermal modeling results show that the tape with electrically conductive acrylic adhesive used in this study is predicted to yield a device operating temperature ranging between  $105^\circ\text{C}$  and  $128^\circ\text{C}$ .

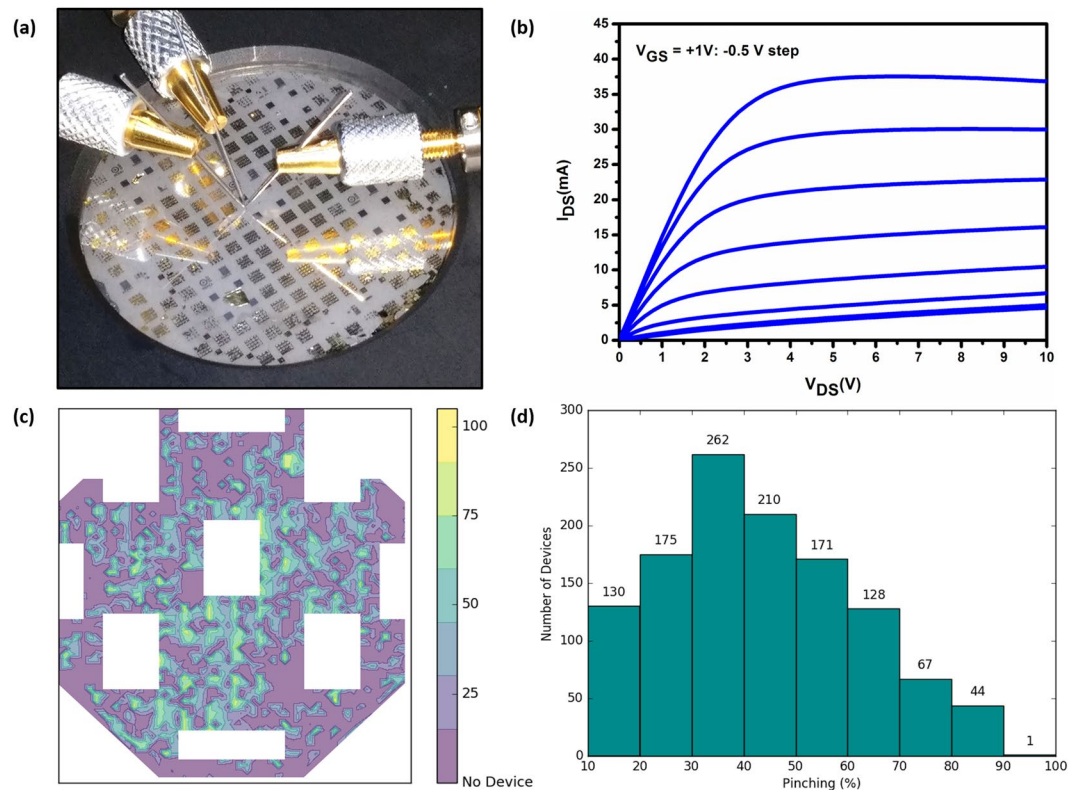


**Figure 3.** (a) Photo of the wafer-scale processed AlGaIn/GaN sensors, (b)  $I_{DS}$ - $V_{DS}$  characteristic of an AlGaIn/GaN device with 2 μm gate length (c) Wafer mapping of the gate pinching, with white areas representing masked-off regions that include TLM patterns (d) Histogram of the pinching distribution across the wafer.

In addition, we have performed Raman spectroscopy measurements on the  $E_2$  GaN line before and after transfer at different temperatures and with different input powers, based on the method reported in ref.<sup>15</sup>. The Raman measurements show that pre-transfer self-heating results in a sensor temperature of 60 °C in the active region. After transfer, the sensor temperature was measured to be 120 °C. These results are consistent with thermal simulations presented in Fig. 5. It also explains the drop in  $I_0$  after transfer since device temperature is inversely related to the electron mobility in the 2DEG<sup>16</sup>.

To verify whether this increase in device operating temperature is the primary reason behind the boosted performances, we have operated a pre-transfer sensor (on h-BN/sapphire) at 120 °C and compared the performance to the transferred sensor. The sensitivity and the response time of a pre-transfer device were measured as a function of temperature. The results show that the sensitivity has only increased by a factor of 1.06 when varying the stage temperature from 30 °C to 120 °C, and the response time has decreased by a factor of 2.47. Because these factors are less than those resulting from the transfer (1.94 and 6.31, respectively), it suggests that other reasons in addition to thermal effects are behind the post-transfer performance enhancement.

The effects from strain changes in the semiconductor layers after the transfer may play a role and should be considered. Raman spectroscopy results, performed at room temperature both before and after transfer, show a relaxation of the GaN layer after the transfer. The  $E_2$  peak of GaN has shifted towards less compressive strains, as presented in Fig. 6a, which agrees with the reported results in ref.<sup>11</sup> and indicates an increase of the 2DEG carrier density. This is necessarily linked with an increase in the surface state charges to maintain the electrostatic neutrality<sup>17</sup>, and can consequently contribute to the enhancement in sensitivity since the gas molecules are chemically absorbed to surface charges after dissociation on the Pt sensing layer<sup>18</sup>.

To further confirm the increase in 2DEG carrier density, we have conducted C-V measurements at different frequencies between the gate and the source of a device before and after its transfer to the adhesive tape. From the C-V profiling in Fig. 6b, we observe a 39% increase in maximum capacitance measured at 1 kHz after transfer which is directly related to the 2DEG carrier density at the AlGaIn/GaN interface.

It is clear that temperature increase and stress release are both valid causes for the performance boost but other effects as surface charge traps density could be also investigated. Another possible factor for the enhanced sensor performance could be related to modification of the strain in the Pt sensing layer during transfer, which is known to change the catalyst efficiency<sup>19,20</sup> and hence it may also contribute to the decreased response time. More in depth study should be carried out to better understand the individual contributions of each of these factors to the total increase of device performance.

In conclusion, we have demonstrated wafer-scale fabrication of AlGaIn/GaN gas sensors grown on an ultra-thin h-BN layer on a 2-inch sapphire substrate. The h-BN layer allowed the transfer of the devices to a flexible and heat insulating acrylic tape. Gas sensing measurements have been carried out before and after the

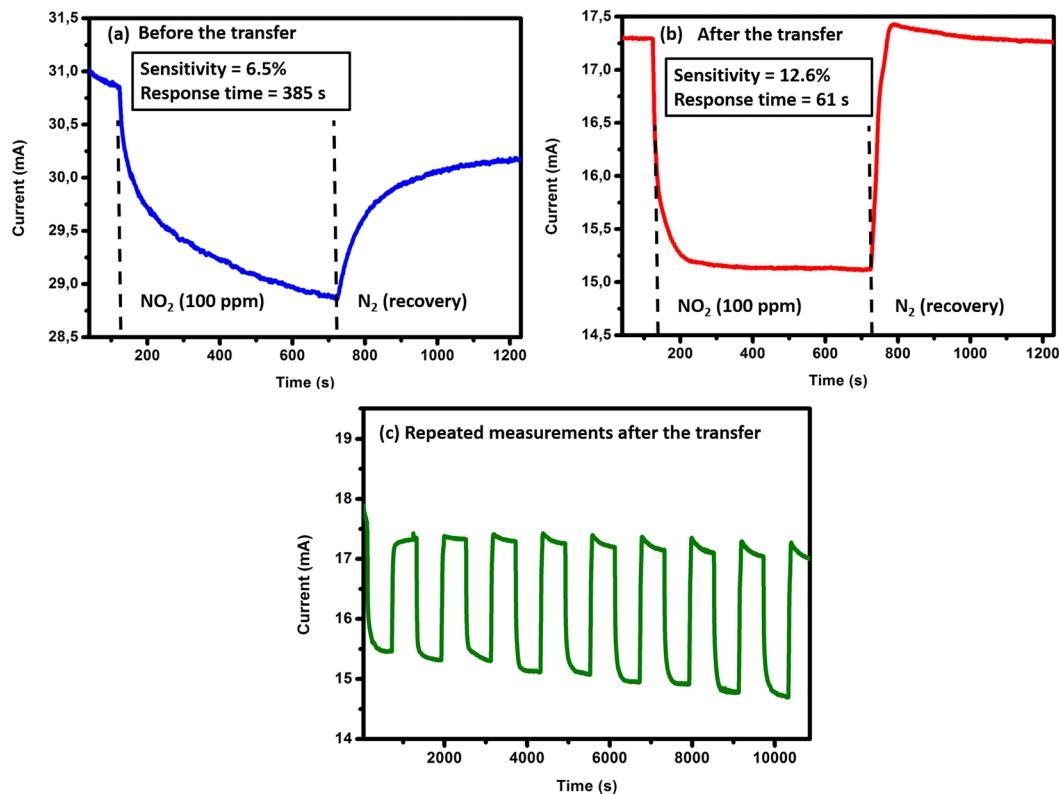


**Figure 4.** Response of an AlGaIn/GaN sensor, with a gate size of  $2\ \mu\text{m} \times 200\ \mu\text{m}$ , to  $\text{NO}_2$  gas for a concentration of 100 ppm at  $30^\circ\text{C}$ . (a) Before the transfer, (b) after the transfer to the flexible template and (c) Repeated measure after the transfer showing the stability of the transferred device after 9 cycles.

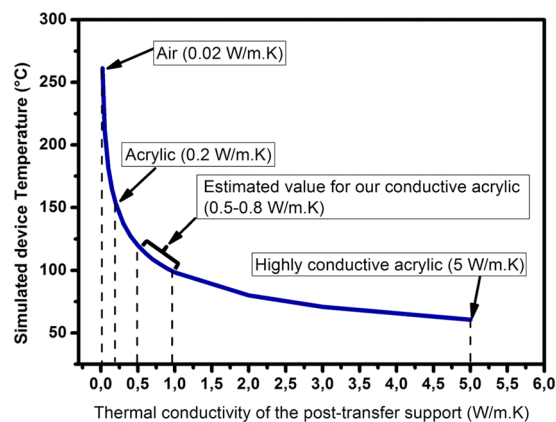


**Figure 5.** Thermal simulation of the operating device temperature Vs thermal conductivities of different post-transfer supports.

transfer showing greatly improved performance on the flexible substrate. We have considered the effects of the post-transfer substrate choice on the device operating temperature which has been shown to increase through Raman spectroscopy and thermal simulations. The boosted sensor performance may also be attributed to structural modifications that increase the number or the accessibility of surface states at the platinum/GaN cap interface and/or enhance the catalytic reaction in the sensing layer. The approach for device engineering demonstrated in this work provides new options towards the development of GaN-based flexible sensors with enhanced device performance, improved economic viability, and an expanded range of applications.

## Methods

**Material growth.** Materials growth was performed in an Aixtron MOVPE CCS  $3 \times 2''$  system on a 2 inch (0001) sapphire substrate. Triethylboron (TEB), Trimethylgallium (TMGa), Trimethylaluminum (TMAI) and Ammonia ( $\text{NH}_3$ ), were used as B, Ga, Al and N sources respectively. First, an h-BN layer (3–5 nm) was grown

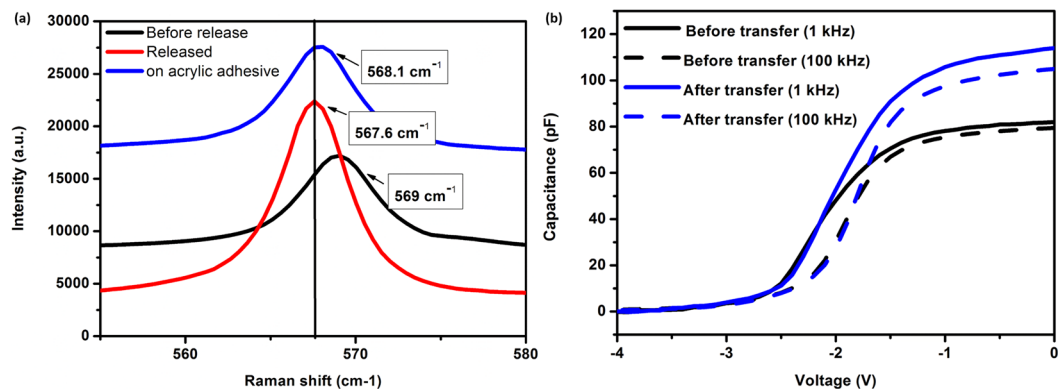


**Figure 6.** (a) Raman spectra at E2 peak of GaN on h-BN/sapphire (black), released from the sapphire (red) and transferred to an adhesive acrylic tape (red). (b) Capacitance-voltage measured at 1 kHz and 100 kHz on a device before and after its transfer. Both Raman and C-V results indicate an increase in the 2DEG density after the release and transfer to the acrylic adhesive tape.

on the sapphire substrate at 1300 °C. Then, a nucleation AlGa<sub>0.14</sub>N layer (250 nm) with an Al mole fraction of 14% was grown at 1100 °C. We subsequently grew an AlGa<sub>0.14</sub>N/GaN heterostructure consisting of a 1- $\mu$ m-thick GaN buffer layer and a 25-nm-thick AlGa<sub>0.14</sub>N barrier layer with an Al composition of 25%, which was confirmed by XRD measurements. Finally, a 3 nm GaN cap layer was grown. High resolution X-ray diffraction (HRXRD) scans were done in Panalytical X'pert Pro MRD system with Cu K $\alpha$  radiation.

**Device processing.** The use of sacrificial h-BN for wafer-scale fabrication of gas sensors poses a processing challenge because spontaneous delamination of the grown structure can occur during device processing when the wafer is subject to various mechanical strains. In our experience, careful control and optimization of each fabrication step is required. The source, drain, and contacts were defined by optical lithography. The deposit of the source and drain metallization contact structure consisted of electron beam evaporated Ti/Al/Ni/Au (12/200/40/100 nm) multilayers followed by a rapid thermal annealing at 870 °C for 30 s under nitrogen atmosphere. The gate contact was deposited using Pt sputtering with a thickness of 15 to 20 nm at a pressure of 6 mTorr, providing a catalytically active sensing layer. Gate dimensions are  $L_g = 2 \mu\text{m}$  and  $W_g = 200 \mu\text{m}$ , with a total drain to source spacing of 6  $\mu\text{m}$ . Electron beam evaporated Ti/Al/Ni/Au (12/200/40/100 nm) pads were deposited to facilitate electrical contacting of the devices.

After sensor processing, electrical characterization was performed using an automated probe station to test the electrical behavior of the devices. Then, the sapphire layer was removed by fixing supports to both the sapphire and active layer sides with a thermoplastic polymer, and applying pressure so that the Van der Waals bonds in the h-BN layer are broken. The active layers are then transferred to a flexible substrate; we have chosen to use a tape with acrylic adhesive for thermal insulation. The top support is removed by heating the thermoplastic at 60 °C and rinsing the residues with DI water.

**Experimental testing of gas sensors.** A subset of the transferred sensor devices has been tested as gas sensors before and after their transfer to copper flexible tape. For experimental testing, the sensors were connected with probes in a gas chamber and linked to a Keithley 236 I-V measurement system. Gas sources of pure N<sub>2</sub> and NO<sub>2</sub> with 100 ppm concentration were supplied to the testing chamber via an MCQ gas mixer utilizing separate mass flow controllers for each gas line. Pressure, concentration, temperature, and flow rate were all controlled and kept constant during the measurements. All experiments were carried out at atmospheric pressure. The substrate temperature was controlled using an external temperature controller with a heater and fixed at 30 °C. A flow rate of 100 sccm was used and with all external factors controlled, we can attribute changes in the steady state signal to the gas detection mechanism described in [2]. For each measurement, the signal under pure N<sub>2</sub> was used as a reference for comparison with the signal under the test gas in a background of nitrogen.

**Thermal modeling.** Thermal simulations have been performed along with the temperature measurements made on pre- and post-transfer devices by means of Raman spectroscopy. One would expect that the primary difference between the two devices would be a higher temperature post-transfer, because of the low thermal conductivity of the 35 micron thick electrically conductive acrylic adhesive between the transferred devices and the copper film. The simulations show that this is the case. In addition, they show that in the vertical direction in the AlGa<sub>0.14</sub>N/GaN structure, the temperature is very nearly uniform, with less than 0.1 °C temperature difference, which implies that the vertically averaged temperature measured by Raman spectroscopy is within 0.1 °C of that of the Pt/AlGa<sub>0.14</sub>N interface. Thermal conductivities used in the simulation are 130 W/m.K for GaN, 25 W/m.K for Al<sub>0.14</sub>Ga<sub>0.86</sub>N, 20 W/m.K for Al<sub>0.25</sub>Ga<sub>0.75</sub>N, 19 W/m.K for Ti, 205 W/m.K for Al, 90 W/m.K for Ni, 314 W/m.K for Au, 72 W/m.K for Pt, and 385 W/m.K for copper. The temperature at the 25-micron thick copper film is 30 °C, the same as the chuck holder.

In simulations, the temperature at the Pt/AlGaN interface on a post-transfer device during 5 V operation depends strongly on the thermal conductivity of the electrically conductive acrylic adhesive. Non-conductive acrylic has a thermal conductivity of approximately 0.2 W/m.K, while the thermal conductivity of commercial conductive acrylic adhesives ranges from 0.5 to 5 W/m.K. As our tape is not meant to be highly thermally conductive, its thermal conductivity is estimated to be between 0.5 and 0.8 W/m.K which is consistent with Raman results.

**Raman spectroscopy.** Raman shift spectra were measured by LabRam HR EVOLUTION Raman spectroscopy with laser excitation at 532 nm. For calibration, the GaN  $E_2$  Raman shift as a function of temperature was measured through the platinum gate on a non-operating sensor before lift-off. The  $E_2$  shift moved from 568.25  $\text{cm}^{-1}$  at 30 C to 564  $\text{cm}^{-1}$  at 300 C in a line. Then with the sample holder set to 30 C, the Raman shift was measured during operation with  $V_{DS} = 5$  V, before and after the transfer.

## References

1. Song, J., Lu, W., Flynn, J. & Brandes, G. Pt-AlGaN/GaN Schottky diodes operated at 800 °C for hydrogen sensing. *Appl. Phys. Lett.* **87**, 133501 (2005).
2. Bishop, C. *et al.* Experimental Study and Device Design of NO, NO<sub>2</sub>, and NH<sub>3</sub> Gas Detection for a Wide Dynamic and Large Temperature Range Using Pt/AlGaN/GaN HEMT. *IEEE Sensors Journal* **16**, 18 (2016).
3. Halfaya, Y. *et al.* Investigation of the Performance of HEMT-Based NO, NO<sub>2</sub> and NH<sub>3</sub> Exhaust Gas Sensors for Automotive Antipollution Systems. *Sensors* **16**(3), 273 (2016).
4. Kelly, M. K. *et al.* Large Free-Standing GaN Substrates by Hydride Vapor Phase Epitaxy and Laser-Induced Liftoff. *Jpn. J. Appl. Phys.* **38**, L217–L219 (1999).
5. Mhedhbi, S. *et al.* Recent improvements of flexible GaN-based HEMT technology. *Phys. Status Solidi A*, 1600484 (2017).
6. Rogers, D. J. *et al.* Use of ZnO thin films as sacrificial templates for metal organic vapor phase epitaxy and chemical lift-off of GaN. *Appl. Phys. Lett.* **91**, 071120 (2007).
7. Utama, M. I. B. *et al.* Recent developments and future directions in the growth of nanostructures by van der Waals epitaxy. *Nanoscale* **5**, 3570 (2013).
8. Kobayashi, Y., Kumakura, K., Akasaka, T. & Makimoto, T. Layered boron nitride as a release layer for mechanical transfer of GaN-based devices. *Nature* **484**, 223 (2012).
9. Taha, Ayari *et al.* Wafer-scale controlled exfoliation of metal organic vapor phase epitaxy grown InGaN/GaN multi quantum well structures using low-tack two-dimensional layered h-BN. *Appl. Phys. Lett.* **108**, 171106 (2016).
10. Alam, Muhammad A. & Kumar, Satish. “Definition of Flexible Electronics,” ed. Bharat Bhushan, Encyclopedia of Nanotechnology (2014).
11. Hiroki, M., Kumakura, K. & Yamamoto, H. Enhancement of performance of AlGaN/GaN high-electron-mobility transistors by transfer from sapphire to a copper plate. *Jpn. J. Appl. Phys.* **55** (2016).
12. Makimoto, T., Kumakura, K., Kobayashi, Y., Akasaka, T. & Yamamoto, H. Suppression of self-heating effect in AlGaN/GaN high electron mobility transistors by substrate-transfer technology using h-BN. *Appl. Phys. Exp.* **5**, 072102 (2012).
13. Li, X. *et al.* Large-Area Two-Dimensional Layered Hexagonal Boron Nitride Grown on Sapphire by Metalorganic Vapor Phase Epitaxy. *Cryst. Growth Des* **16**, 3409–3415 (2016).
14. Ahmed, K. *et al.* Solid-state neutron detectors based on thickness scalable hexagonal boron nitride. *Appl. Phys. Lett.* **110**, 023503 (2017).
15. Nazari, M., Hancock, B. L., Piner, E. L. & Holtz, M. W. Self-Heating in a GaN-Based Heterojunction Field-Effect Transistor Investigated by Ultraviolet and Visible Micro-Raman Spectroscopy. Compound Semiconductor Integrated Circuit Symposium (CSICS), IEEE (2015).
16. Gaska, R. *et al.* Electron transport in AlGaN–GaN heterostructures grown on 6H–SiC substrates. *Appl. Phys. Lett.* **72**(6), 707–709 (1998).
17. Anwar, A. F. M. & Faraclas, E. W. Schottky barrier height in GaN/AlGaN heterostructures. *Solid-State Electronics* **50**, 1041 (2006).
18. Ali, M. *et al.* Pt/GaN Schottky diodes for hydrogen gas sensors. *Sensors and Actuators B* **113**, 797–804 (2006).
19. Bu, L. *et al.* Biaxially strained PtPb/Pt core/shell nanoplate boosts oxygen reduction catalysis. *Science* **354**, 1410–1414 (2016).
20. Wang, H. *et al.* Direct and continuous strain control of catalysts with tunable battery electrode materials. *Science* **354**, 1031–1036 (2016).

## Acknowledgements

This study has been partially funded by the French National Research Agency (ANR) under the GANEX Laboratory of Excellence (Labex) project. The authors would like to thank T. Kauffmann from LMOPS, a lab operated by both Université de Lorraine and CentraleSupélec, for his help on Raman spectroscopy measurements. The authors would like also to thank Y. Halfaya from CEA-Tech for his help on the C-V measurements. The author G.P. acknowledges the French National Research Agency for the project TEMPOS (ANR-10-EQPX-50) in the framework of the “Future Investments” program.

## Author Contributions

A.O. contributed to design the study and supervised the whole project. T.A. performed Raman, device fabrication, electrical measurements and gas test experiments. C.B. designed the contact pattern for the device and the gas test setup. T.A. and C.B. wrote the manuscript. S.S., X.L. and S.A. optimized the growth parameters and prepared the samples. Y.E.G. carried out XRD measurements. J.-P.S., M.B.J. were responsible for the processing and electrical tests. P.L.V. carried out the thermal simulations. G.P. performed the HRTEM experiments. All authors contributed to discussions of the results. All authors reviewed and commented on the manuscript.

## Additional Information

**Competing Interests:** The authors declare that they have no competing interests.

**Publisher's note:** Springer Nature remains neutral with regard to jurisdictional claims in published maps and institutional affiliations.



**Open Access** This article is licensed under a Creative Commons Attribution 4.0 International License, which permits use, sharing, adaptation, distribution and reproduction in any medium or format, as long as you give appropriate credit to the original author(s) and the source, provide a link to the Creative Commons license, and indicate if changes were made. The images or other third party material in this article are included in the article's Creative Commons license, unless indicated otherwise in a credit line to the material. If material is not included in the article's Creative Commons license and your intended use is not permitted by statutory regulation or exceeds the permitted use, you will need to obtain permission directly from the copyright holder. To view a copy of this license, visit <http://creativecommons.org/licenses/by/4.0/>.

© The Author(s) 2017